Electrocochleographic frequency-following responses as a potential marker of age-related cochlear neural degeneration

Temboury-Gutierrez, Miguel; Märcher-Rørsted, Jonatan; Bille, Michael; Yde, Jesper; Encina-Llamas, Gerard; Hjortkjær, Jens; Dau, Torsten

Published in:
Hearing Research

Link to article, DOI:
10.1016/j.heares.2024.109005

Publication date:
2024

Document Version
Publisher's PDF, also known as Version of record

Hearing Research 446 (2024) 109005

Contents lists available at ScienceDirect

Hearing Research

journal homepage: www.elsevier.com/locate/heares

Research Paper

Electrocochleographic frequency-following responses as a potential marker of age-related cochlear neural degeneration☆,☆☆

Miguel Temboury-Gutierrez [a,*], Jonatan Märcher-Rørsted [a], Michael Bille [b], Jesper Yde [b], Gerard Encina-Llamas [a,b,c], Jens Hjortkjær [a,d], Torsten Dau [a]

[a] Hearing Systems Section, Department of Health Technology, Technical University of Denmark, Ørsteds Plads, Building 352, DK-2800 Kgs. Lyngby, Denmark
[b] Copenhagen Hearing and Balance Center, Ear, Nose and Throat (ENT) and Audiology Clinic, Rigshospitalet, Copenhagen University Hospital, Denmark, Inge Lehmanns Vej 8, DK-2100 København Ø, Denmark
[c] Faculty of Medicine. University of Vic – Central University of Catalonia (UVic-UCC), Vic, 08500, Catalonia - Spain
[d] Danish Research Centre for Magnetic Resonance, Centre for Functional and Diagnostic Imaging and Research, Copenhagen University Hospital Hvidovre, Kettegård Allé 30, DK-2650 Hvidovre, Denmark

ARTICLE INFO

Keywords:
Age-related hearing loss
Cochlear synaptopathy
Frequency-following response
Electrocochleography
Auditory nerve neurophonic

ABSTRACT

Auditory nerve (AN) fibers that innervate inner hair cells in the cochlea degenerate with advancing age. It has been proposed that age-related reductions in brainstem frequency-following responses (FFR) to the carrier of low-frequency, high-intensity pure tones may partially reflect this neural loss in the cochlea (Märcher-Rørsted et al., 2022). If the loss of AN fibers is the primary factor contributing to age-related changes in the brainstem FFR, then the FFR could serve as an indicator of cochlear neural degeneration. In this study, we employed electrocochleography (ECochG) to investigate the effects of age on frequency-following neurophonic potentials, i.e., neural responses phase-locked to the carrier frequency of the tone stimulus. We compared these findings to the brainstem-generated FFRs obtained simultaneously using the same stimulation. We conducted recordings in young and older individuals with normal hearing. Responses to pure tones (250 ms, 516 and 1086 Hz, 85 dB SPL) and clicks were recorded using both ECochG at the tympanic membrane and traditional scalp electroencephalographic (EEG) recordings of the FFR. Distortion product otoacoustic emissions (DPOAE) were also collected. In the ECochG recordings, sustained AN neurophonic (ANN) responses to tonal stimulation, as well as the click-evoked compound action potential (CAP) of the AN, were significantly reduced in the older listeners compared to young controls, despite normal audiometric thresholds. In the EEG recordings, brainstem FFRs to the same tone stimulation were also diminished in the older participants. Unlike the reduced AN CAP response, the transient-evoked wave-V remained unaffected. These findings could indicate that a decreased number of AN fibers contributes to the response in the older participants. The results suggest that the scalp-recorded FFR, as opposed to the clinical standard wave-V of the auditory brainstem response, may serve as a more reliable indicator of age-related cochlear neural degeneration.

1. Introduction

Aging is associated with degeneration of the peripheral auditory system, although some cochlear structures may be more susceptible to age-related changes than others. Histopathological studies of human temporal bones have shown that aging is associated with a progressive loss of hair cells and auditory nerve fibers (ANF), as well as a degeneration of the stria vascularis (Wu et al., 2019). The loss of outer hair cells (OHC) is associated with an increase in pure-tone audiometric thresholds (Ryan and Dallos, 1975), which have been considered the gold-standard test in audiological assessment. However, pure-tone audiometry is largely insensitive to other types of losses, such as IHC loss (Lobarinas et al., 2013) or ANF loss (Schuknecht and Woellner, 1955). In recent years, various electroencephalographic (EEG) responses

☆ **ABBREVIATIONS:** (that are not standard in this field) None.☆☆ Part of this work was presented at the 24th International Congress on Acoustics, "Electrocochleographic frequency following responses as a potential marker of age-related peripheral degeneration".

* Corresponding author at: Hearing Systems Section, Department of Health Technology, Technical University of Denmark, Ørsteds Plads, Building 352, 2800 Kgs. Lyngby, Denmark.
E-mail address: mtegu@dtu.dk (M. Temboury-Gutierrez).

https://doi.org/10.1016/j.heares.2024.109005
Received 23 November 2023; Received in revised form 19 March 2024; Accepted 1 April 2024
Available online 4 April 2024

have been proposed and investigated as potential markers to estimate the degree of auditory nerve (AN) degeneration or cochlear synaptopathy (CS), i.e., the disruption of synaptic connections between ANFs and IHCs in the cochlea (Bharadwaj et al., 2015; Encina-Llamas et al., 2019; Keshishzadeh et al., 2021; Kujawa and Liberman, 2009; Liberman et al., 2016; Mehraei et al., 2016; Sergeyenko et al., 2013). Furthermore, computer model simulations have suggested that frequency-following responses (FFR) to low-frequency pure tones could be sensitive to AN loss independent of the status of OHCs (Märcher-Rørsted et al., 2022). Consistent with these findings, studies have demonstrated a reduction in brainstem FFRs elicited by low-to-mid frequency (i.e., 100–1000 Hz) periodic stimuli among older participants (Clinard and Cotter, 2015; T. A. Johnson and Brown, 2005; Vander Werff and Burns, 2011), including those with clinically-normal or near-normal audiometric thresholds (Anderson et al., 2012; Mamo et al., 2016; Märcher-Rørsted et al., 2022; Presacco et al., 2016). However, age-related deficits in central auditory processing, such as neural desynchronization at the auditory brainstem level (Pichora-Fuller et al., 2007; Robert Frisina and Frisina, 1997; Schneider et al., 1998), may also contribute to the decline in FFRs associated with aging. Furthermore, the relative contributions of peripheral and central effects on FFR reduction are not well understood. To further investigate this, the present study pursued a direct comparison of centrally-generated FFRs with the synchronized population response generated at the level of the AN (known as the auditory nerve neurophonic, ANN).

CS and AN degeneration have been extensively studied in animal models, focusing on both aging (e.g., Parthasarathy and Kujawa, 2018; Ruan et al., 2014; Sergeyenko et al., 2013) and noise exposure (e.g., Liberman and Kujawa, 2017). In these animal models, noise-induced CS is associated with a decrease in the amplitude of the compound action potential (CAP) or the wave I of the auditory brainstem response (ABR) in response to transient, high-intensity stimuli. Histological assessments of synapse counts and the amplitude of suprathreshold CAP or ABR wave I have shown strong correlations in mouse, guinea pig, chinchilla and rat models (see Hickox et al., 2017 for a comprehensive review). The amplitude of the ABR wave I has also been considered as a potential diagnostic marker of age-related or noise-induced ANF loss in humans (Carcagno and Plack, 2020; Garrett and Verhulst, 2019; Grant et al., 2020; Guest et al., 2017; Prendergast et al., 2019). In aging, cochlear synaptic loss in humans is likely to co-occur with other cochlear pathologies, such as OHC loss, which also impact the amplitude of the ABR wave I, and the sensitivity of this measure for CS in humans is therefore still a topic of debate (Bramhall et al., 2019). It has been argued that basal (Elberling, 1974), high-spontaneous rate (Bourien et al., 2014) ANFs are the primary contributors to the CAP or ABR wave-I amplitude and in older humans, this cochlear region exhibits a combination of significant losses of IHCs, OHCs and AN synapses (Wu et al., 2021). Consequently, ABR wave-I amplitudes in humans may lack specificity since a combination of different peripheral damages can all lead to a reduction in this measure. While there have been attempts to distinguish neural from presynaptic elements by separating superimposed potentials or adjusting for hearing thresholds in statistical models (P. Johannesen et al., 2019; Vasilkov et al., 2023), the effectiveness of these efforts remains uncertain. The degree to which hair cell potentials overlap with the spiking component of wave I is unclear (Lutz et al., 2022, their Figure 7B). Moreover, adjusting for thresholds assumes a linear relation between OHC loss and peak amplitudes, while overlooking the impact of other cochlear degeneration, such as strial degeneration or IHC dysfunction. Additionally, quantifying and differentiating the effects of accumulated noise exposure from the effects of natural aging in human listeners is challenging.

ABRs, measured using scalp EEG and transient stimuli such as clicks, short tones or fast chirps, consist of multiple wave peaks, each associated with a specific latency. The sequential peaks are believed to represent evoked neuronal activity at different generators along the auditory pathway. The first wave in the ABR (wave I) is generated by the population response of the AN (Ferraro, 1998). Waves III through V are thought to originate from more central ascending auditory nuclei, including the cochlear nucleus (CN) and the inferior colliculus (IC) (Møller et al., 1988). Wave-I amplitude of the ABR is generally observed only with high-intensity stimuli that activate a sufficient number of ANFs synchronously (Dau et al., 2000). However, even with high-intensity stimulation, identifying these responses can be challenging in clinical procedures with limited time constraints (e.g., Steinhoff et al., 1988). On the other hand, the amplitude of the brainstem-generated ABR wave V is a more robust measure and can typically be identified even at stimulation levels close to the hearing threshold (Hecox and Galambos, 1974). However, studies in humans have shown that the reduction in wave-I amplitude with age is not mirrored by changes in wave-V amplitude (Burkard and Sims, 2001; Johannesen et al., 2019; Moosavi et al., 2016). This lack of reduction in wave-V amplitude in older listeners (Grose et al., 2019; Rumschlag et al., 2022) may be attributed to a form of gain compensation occurring at the brainstem level in response to degraded peripheral input (e.g., Auerbach et al., 2014; Salvi et al., 2017; Sheppard et al., 2018).

In the case of FFRs, sustained acoustic stimulation (such as a tone) elicits synchronized population responses at various stages along the auditory pathway. However, due to the temporal overlap of these responses, it becomes more challenging to distinguish the specific sources of the scalp FFR (Gardi et al., 1979). Within the cochlea, presynaptic sources generate sustained 'microphonic' responses (the cochlear microphonic, CM), thought to mainly originate from cochlear OHCs. 'Neurophonic' responses following stimulus periodicities can be recorded along the auditory pathway, including the AN, the cochlear nuclei, the medial superior olive (MSO), the IC, and the auditory cortex (Worden and Marsh, 1968). It is commonly assumed that the ascending auditory system exhibits a low-pass characteristic, as the tendency to phase lock to fast fluctuations declines towards the cortex. While AN fibers can phase lock to frequencies in the several thousands of Hz range (Dynes and Delgutte, 1992; D. H. Johnson, 1980), neurons in the rostral brainstem are estimated to show phase locking up to approximately 1 kHz (Bidelman, 2015; Liu et al., 2006) with the most prominent range being in the hundreds of Hz. Since different neural generators have varying phase-locking limits, higher stimulation frequencies can be utilized to elicit phase-locked responses predominately driven by earlier neural sources. Furthermore, different scalp electrode configurations can optimize or minimize the contributions of different nuclei (e.g., King et al., 2016). In this study, we leverage this low-pass frequency dependence and sensitivity to electrode placement to help differentiate peripheral from central contributions.

When narrowband stimuli are presented at high intensities, they result in a broad excitation across AN fibers. In the context of eliciting an FFR, low-frequency tones with high intensities lead to a spread of excitation in the cochlea and synchronized basal (i.e., off-frequency) AN responses which significantly contribute to the (more broadband) gross potential (Dau, 2003; Encina-Llamas et al., 2019). Dysfunction or loss of OHCs limited to frequencies above the frequency of stimulation, as observed in 'normal-aging' adults (Wu et al., 2019), does not result in a reduction of the more broadband AN response to the low-frequency, high-intensity stimuli (Märcher-Rørsted et al., 2022). OHC loss should therefore not diminish the peripheral component of the FFR (i.e., the ANN). Model simulations suggest that the ANN response to periodic low-frequency, high-intensity stimuli is robust against mid-to-high-frequency OHC loss, while it remains sensitive to broadband IHC loss and deafferentation (i.e., CS) (Märcher-Rørsted et al., 2022). This resilience to high-frequency OHC loss may offer an advantage in utilizing the FFR as a marker of AN degeneration compared to the ABR.

In this study, we conducted measurements of both sustained and transient-evoked potentials in young and older participants with near-normal hearing thresholds. To elicit responses dominated by either peripheral or central sources, we employed ECochG and EEG recording

montages while measuring sustained responses to different tone carrier frequencies. The stimulation was performed at moderately-high sound pressure levels (85 dB SPL) using 250-ms long pure tones, allowing comparison with previous studies that utilized similar stimulus and level conditions (Clinard et al., 2010; Krishnan and Mcdaniel, 1998; Märcher-Rørsted et al., 2022; Marmel et al., 2013). Additionally, we recorded responses to high-intensity (100 dB peak-to-peak equivalent SPL) 10-ms tone pulses, aiming to activate a large population of ANFs for better identification of onset and offset latencies and their associations with different response generators. Furthermore, we aimed to assess the significance of potential contributions from pre-synaptic sources by employing a tone at a higher frequency (3096 Hz), i.e., beyond the limit of neural phase locking. By using the different recording montages and stimulation frequencies, we investigated whether age-related reductions in brainstem FFRs would be accompanied by reductions in cochlear neurophonic responses to the same stimulation. Such findings would help disentangle the role of age-related ANF loss in the known reduction of brainstem-generated FFR observed in older adults.

2. Materials and methods

2.1. Participants

Twenty-nine subjects participated in the study. The participants were recruited based on age and audiometric sensitivity ($\leq$ 25 dB hearing level (HL) from 125 Hz to 6 kHz) and divided into a young group ($n = 15$, ages 20–31 years, mean age 23.5 $\pm$ 3 years, 5 men) and an older group ($n = 14$, ages 58–79 years, mean age 64.7 $\pm$ 7.1 years, 5 men). One young, female participant was excluded from the data analysis due to excessive noise present in all recordings, leaving 14 participants in each group. To verify the audiometric thresholds used to recruit the participants, we measured air conduction thresholds from 125 Hz to 8 kHz using IP30 insert earphones (RadioEar) as well as extended high frequency (EHF) thresholds with pure tones from 10 to 16 kHz, using DD450 circumaural headphones (RadioEar). The ear that exhibited the lowest average audiometric thresholds (pure-tone average from 125 Hz to 6 Hz) or met the criterion of $\leq$ 25 dB HL from 0.125 to 6 kHz, was selected as the "test ear" and used for subsequent measurements. The thresholds of both ears were within a 20 dB range at each measured frequency from 125 Hz to 4 kHz for all participants. The experiment was conducted over two sessions. In the first session, which lasted one hour, audiometry and DPOAEs were obtained. The second session, lasting two hours, was dedicated to collecting the electrophysiological measurements. Written consent was obtained from all participants to take part in the study, which was approved by the Science Ethics Committee of the Capital Region of Denmark (protocol H-21,049,895). The study was conducted in compliance with the Declaration of Helsinki. All measurements were conducted at the Copenhagen Hearing and Balance Center at Rigshospitalet in Copenhagen, Denmark.

2.2. Distortion product otoacoustic emissions (DPOAE)

To assess OHC status, DPOAEs were assessed in the participants' test ear using the Interacoustics Titan system. Two pure tones, known as primaries (F1 and F2), were used for the DPOAE measurements, with a fixed ratio (F2/F1) of 1.22. The level difference between the primaries was set at 10 dB, such that F2 = F1 – 10 dB. DPOAE amplitudes were evaluated at the distortion product frequency of 2F1-F2. Both frequency-dependent (500 Hz to 10 kHz at F1=65 dB SPL) and level-dependent (at F1=40 to 65 dB SPL, in 5 dB steps, for 1, 3, 8 and 10 kHz) DPOAEs were measured. In the frequency-dependent measurements, the levels of the two primaries were kept constant (F1 at 65 dB SPL and F2 at 55 dB SPL), while the frequency of F2 varied across different frequencies (0.5, 1, 1.5, 2, 3, 4, 5, 6, 7, 8, 9, 10 kHz). For the level-dependent DPOAEs, measurements were taken at two frequencies also used for the electrophysiological measurements (F2 = 1032 and 3096 Hz) to account for potential localized OHC dysfunction. Additionally, two higher frequencies (F2 = 8 and 10 kHz) were included to assess the condition of basal OHCs.

2.3. Electrophysiology

2.3.1. Stimuli

Transient-evoked potentials were recorded in response to 100-μs clicks presented at a level of 115.5 dB ppeSPL. The clicks were jittered and presented at two different rates: 12 Hz and 40 Hz. Each presentation rate involved 6000 clicks, alternating in polarity. To elicit the ANN and FFR, tone pulses of 250-ms duration (with a 1-ms rise/fall sinusoidal ramp) were presented at 516 and 1086 Hz. The stimulus intensity was set at 85 dB SPL, and 500 repetitions were presented for each polarity at a rate of 2 Hz. Additionally, to assess the ANN and FFR at higher stimulation levels, 10-ms tone pulses (with a 1-ms rise/fall sinusoidal ramp) were presented at 516, 1032 and 3096 Hz, at a level of 100 dB ppeSPL. The tone pulses at different frequencies were jittered and presented separately at 12 Hz with 3000 repetitions for each onset polarity.[1] All stimuli were presented monaurally using ER-3 insert earphones. The earphones were placed in custom-made metal boxes to minimize electrical noise, and the cables connecting the earphones to the soundcard were electrically shielded. To avoid additional electric artifacts, the inner part of the box was soldered to an extra cable connected to ground outside of the booth. The entire stimulation paradigm lasted one hour, and participants were given 5-minute breaks between recordings obtained with the different stimuli (clicks, long tone pulses, and short tone pulses).

2.3.2. Data acquisition

Electrophysiological data were recorded using the BioSemi ActiveTwo system at a sampling frequency of 16,384 Hz. The ground electrode with the BioSemi ActiveTwo system consisted of the common mode sense (CMS) and the driven right leg (DRL) electrodes, which were placed on C1 and C2, respectively. Electrophysiological data (EEG and ECochG) were continuously recorded using the ABR module of the ActiveTwo AD box, which offers improved SNRs compared to the traditional BioSemi inputs. The participants were positioned on a bed inside a double-walled, sound-treated, electromagnetically-shielded booth and were instructed to keep their eyes closed, encouraging them to sleep or relax.

2.3.3. Electroencephalography (EEG) setup

EEG measurements were taken using two inputs to the ABR module from BioSemi's ActiveTwo AD box. Neurology surface electrodes (Ambu Neuroline 720) were placed on the ipsilateral mastoid (inverting, P9 or P10) and on the lower forehead (reference, FPz). The skin was disinfected with 85% ethanol prior to electrode application.

2.3.4. Electrocochleography (ECochG) setup

To record cochlear potentials, a TM electrode (Sanibel) connected to the remaining input of the ABR module was placed in the participants' test ear. First, a trained medical doctor inspected the ear canal using an otomicroscope. Liquid local anesthesia (Xylocaine, lidocaine) was then applied, and the tip of the TM electrode was immersed in conductive gel (Signagel, Parker Laboratories) for 10 min. Afterward, the anesthetic was removed from the ear canal using microsuction. The TM electrode was positioned on the tympanic membrane by the medical doctor and secured in place with a foam ER-3 insert tip, which was later connected to the sound delivery system. The correct positioning of the electrode was confirmed by visually inspecting the continuous electrical activity after insertion. The TM electrode's influence on audiometric thresholds

[1] The polarities for the pure tones were presented in different blocks, i.e., not in a true alternating manner.

was confirmed to be negligible (<5 dB) at the frequencies of electrophysiological stimulation (0.5, 1, and 3 kHz) by conducting audiometric tests before and after insertion on a subset of participants (as in Smith et al., 2016).

2.3.5. Data pre-processing

The continuous electrophysiological data underwent automatic high-pass filtering at 100 Hz, by the built-in ABR module of the BioSemi system. MATLAB and the FieldTrip Toolbox (Oostenveld et al., 2011) were used for data pre-processing. During this stage, trial labels and channels were extracted, and a comb-notch filter was applied at 50 Hz and its harmonics up to 1500 Hz to eliminate line noise. The data were then segmented into epochs: from 10 ms before stimulation to 50 ms after stimulation for clicks and 10-ms tone bursts, and from −100 ms to 500 ms for 250-ms tone bursts. Epochs with values exceeding 90 mV, on average 0.22% of the trials, were excluded from further analysis. The remaining epochs were weighted by their inverse variance (Ryan and Dallos, 1975). Polarity-dependent ((C-R)/2) responses to pure tones and polarity-independent ((C + R)/2) responses to clicks were obtained by averaging the polarities. The average responses were band-pass filtered between 100 and 4000 Hz (IIR filter, order 6). Acoustic delay in the sound delivery system (1 ms), was compensated for in all subsequent analyses.

2.3.6. Analysis of transient potentials (CAP and ABR)

We sought to isolate peripheral activity (from the AN) from central activity (from the brainstem) in response to transient and periodic stimuli. As a measure of peripheral synchronized neural activity to transient stimuli, the compound action potential (CAP) N1 peak was extracted from the ECochG configuration (ipsilateral TM-to-mastoid electrode) in response to 12-Hz and 40-Hz rate clicks. For the 40-Hz condition, the CAP amplitude was significantly reduced compared to the 12-Hz condition across all participants (*t*-test, $t(36.5) = 2.90$, $p = 0.013$), reflecting an effect of neural adaptation (Kiang, 1965; Pérez-González and Malmierca, 2014; Sumner and Palmer, 2012). The SP amplitude showed no significant differences between the 12-Hz and the 40-Hz conditions across all participants ($t(47.9) = -0.19$, $p = 0.85$), consistent with results from previous studies (Grant et al., 2020; Liberman et al., 2016). The CAP parameters extracted included onset latency, peak latency, peak amplitude, trough amplitude, and half-width latency, following the approach in (Harris et al., 2021). The modified version of the *localpeak()* function in the ERPlab toolbox (Lopez-Calderon and Luck, 2014) was used to obtain peak latency, peak amplitude, trough amplitude and onset latency. This function searches for the local maxima between 0 and 3 ms of the responses. Additionally, for participants where the SP was detectable, the latency and peak of the SP were obtained using the same modified function. Amplitudes were measured from peak to trough, and the responses were baseline corrected by computing the average of the 2 ms segment preceding the onset of stimulation. The amplitudes and latencies obtained from the function were visually inspected and corrected if necessary, using the ABR wave-I waveform as a reference. The half-width latency was calculated as the latency from the onset of the peak to the peak of the CAP.

As a measure of synchronized central activity, ABRs were recorded in response to the same clicks using the classic ABR ipsilateral mastoid-to-forehead EEG configuration. Like the CAP analysis, onset latency, peak latency and peak amplitude of wave V were estimated using limits of 4.5–6.5 ms (Jerger and Johnson, 1988; Lightfoot, 1993). The function's output was confirmed through visual inspection. Instances where the maxima were inaccurately attributed to the interval limits (4.5 or 6.5 ms) were corrected by reducing the search interval around the peak of the response. Additionally, the phase locking value (PLV) of the response, indicating the level of neural synchrony across epochs, was computed. The PLV was derived using the expression (Delorme and Makeig, 2004):

$$PLV(f,t) = \frac{1}{n}\sum_{k=1}^{n}\frac{F_k(f,t)}{|F_k(f,t)|}$$

where $F_k(f,t)$ represents the complex spectral estimate at time t and frequency f of epoch k. The PLVs range from 0 (indicating complete desynchronization) to 1 (indicating complete synchronization). The time-frequency analysis was performed using the *newtimef()* function from the EEGlab toolbox, employing Hanning tapers, a window size of 32 samples, a pad ratio of 2, and 20 linearly-spaced frequencies ranging from 250 to 5120 Hz. The PLV was then determined as the maximum value within the 2-ms windows surrounding the two peaks (CAP and w-V).

2.3.7. Analysis of sustained potentials (ANN and FFR)

We recorded ANNs and FFRs in response to longer-duration (250 ms) mid-intensity tone pulses (85 dB SPL) and to short (10 ms) high-intensity (100 dB ppeSPL) tone pulses. The magnitudes of the polarity-dependent responses ((C-R)/2) were estimated in the frequency domain at the bin corresponding to the stimulus frequency. This was achieved by computing the spectrum of the response between 0 and 12 ms for the 10-ms tone pulses and between 0 and 250 ms for the 250-ms tone pulses. We calculated the spectral SNR of the electrophysiological signal at the stimulus frequency. The spectral magnitude of the carrier frequency was identified and compared to the surrounding noise floor within a range of ±20 Hz. For the broader spectral peak of the response to the short tone pulses, the noise floor was estimated using 200 Hz (100 Hz on each side) at 100 ± 100 Hz above and below the stimulus frequency. The SNR was computed by dividing the power of the target magnitude bin by the average of the surrounding frequency bins. The probability of the response power being different from the surrounding noise floor was calculated using an F-statistic test (Dobie and Wilson, 1996). FFR measurements were considered statistically significant if $p \leq 0.01$ (1%). For the long tones, 10.7% of the responses from older participants were non-significant, and all responses from young participants were significant. For the shorter tones, 7.1% and 16.7% of the responses from the young and older participants, respectively, were non-significant. Non-significant responses were excluded from the statistical analysis. The amplitudes of the responses were estimated in the frequency domain, by applying the Fast Fourier Transform (FFT) to the averaged response from 0 to 250 ms (for the longer-duration tone pulses) and from 0 to 12 ms (for the short tone pulses) post onset, and evaluating the spectral energy at the frequency bin of stimulation. In Fig. 4, individual ANNs were aligned or 'delay-corrected' for each participant before averaging to facilitate visualization of the waveforms in the time domain. The response delay for each participant was determined by finding the maximum cross-correlation between the response and the stimulus waveforms.

As an additional measure of synchronized activity in the response, we calculated the PLV by averaging the PLVs of the 0-to-12 ms and 0-to-250 ms responses for the short and long tone pulses at each frequency of stimulation. To evaluate potential changes in PLV across the stimulation period, we calculated the PLV in 4 ms long Hann windows (1 ms overlap) from 100 ms before to 250 ms after stimulation onset.

2.4. Statistical tests

We examined differences in the data obtained across participant groups, electrode montages, presentation rates, audiometric pure-tone average (PTA) thresholds, and DPOAE amplitudes using unpaired sample *t*-tests. The results were adjusted for multiple comparisons using Benjamini-Hochberg correction (false discovery rate, FDR) as described by Benjamini & Hochberg (1995). The normality of the data was assessed by examining the normal Q-Q plots (qqnorm and qqline) of the model's residuals. In post-hoc analyses, we included low frequency (<6 kHz) PTA thresholds or DPOAEs (<6 kHz at F1=65 dB SPL) in separate

linear regression models with age as a continuous predictor variable to further investigate effects of age on the long-tone FFRs after accounting for measures mainly reflecting OHC status (i.e., $FFR_{SNR} \sim age + PTA$ and $FFR_{SNR} \sim age + DPOAE$). The linear models were conducted on the SNRs at 516 and 1086 Hz, for both the peripheral (ANN) and brainstem (FFR) electrode setups. All statistical analyses were conducted using R.

3. Results

3.1. Click and tone-pulse responses at peripheral and brainstem level

We first investigated general properties of the different click and tone responses in the different electrode configurations averaged across the younger and older participants. Fig. 1 illustrates the three different types of stimuli (Fig. 1A) and the grand average responses across all participants recorded in the EEG (ipsilateral mastoid-to-vertex Fig. 1B) and ECochG (ipsilateral TM-to-mastoid Fig. 1C) electrode configurations.

The top panel of Fig. 1B displays the across-group average ABR responses to 100-μs, 115.5-dB-ppeSPL clicks presented at 12-Hz, recorded using the EEG mastoid-to-vertex configuration (i.e., ipsilateral mastoid and vertex electrodes). We observed the distinctive response peaks of the ABR, i.e., the SP as well as waves I, III and V. The middle panel of Fig. 1B, shows the grand average FFR to the short 10-ms, 516 Hz tone at 100 dB ppeSPL in the same EEG configuration. As can be seen, the response shows phase locking to the tone frequency, with the response onset aligning with the click ABR wave-III and offset around 15 ms after stimulation onset (indicated by thick dashed lines in Fig. 1B), indicating a brainstem source. The bottom panel of Fig. 1B presents the grand average FFR to the 250-ms, 516-Hz tone at 85 dB SPL. The onset aligns with wave-V of the click response, again indicating a response dominated by brainstem activity.

Responses recorded in the ECochG montage (TM-to-mastoid) are shown in Fig. 1C. The top panel of Fig. 1C shows the click-evoked responses. As can be seen, the response is dominated by the compound action potential (CAP), i.e., the first wave of the click-evoked TM response. The CAP shows a clear SP component, and the SP could more readily be detected with an automated peak detection procedure (see Section 2.3) in individual subjects compared to the mastoid-to-vertex montage (TM: 25; vertex: 15). Later potentials observed in the mastoid-to-vertex montage (i.e., waves III-V) were not clearly present in the TM-to-mastoid montage since peripheral sources (i.e., OHC and AN) dominate this response. The middle and bottom panels in Fig. 1C show the across-group average recorded responses to the 516-Hz, 10-ms tone pulse at 100-dB-ppeSPL and the 516-Hz 250-ms tone pulse at 85-dB-SPL, respectively, recorded at the TM electrode. Here, the onset of the phase-locked responses aligns with the latency of wave I and has a duration of 10 ms (matching the stimulus duration) consistent with a phase-locked AN response (i.e., an ANN). The observed responses in this configuration generally exhibit larger amplitudes than those obtained with the mastoid-to-vertex configuration, consistent with larger click- evoked CAP/wave I amplitudes.

3.2. Audiometry and click-evoked responses

Fig. 2A shows the pure-tone thresholds for the young (blue) and older (red) participants. All participants had audiometric thresholds below 25 dB HL up to 6 kHz. Although the audiometric thresholds were clinically near-normal for all participants, we found statistically significant differences in the clinical frequency range between the two groups (PTA from 125 Hz to 6 kHz, $t(20.0) = -3.21$, $p = 0.011$), with higher thresholds in the older group. At extended high frequencies ($\geq$ 8 kHz), significant differences were observed between the young and older groups (PTA from 8 kHz to 16 kHz, $t(25.4) = -10.6$, $p = 4.7e\text{-}10$). Importantly, there were no significant threshold differences between the groups at 500 Hz ($t(17.8) = -1.8$, $p = 0.089$), ensuring that the audibility of the lowest frequency used for tonal stimulation (516 Hz)

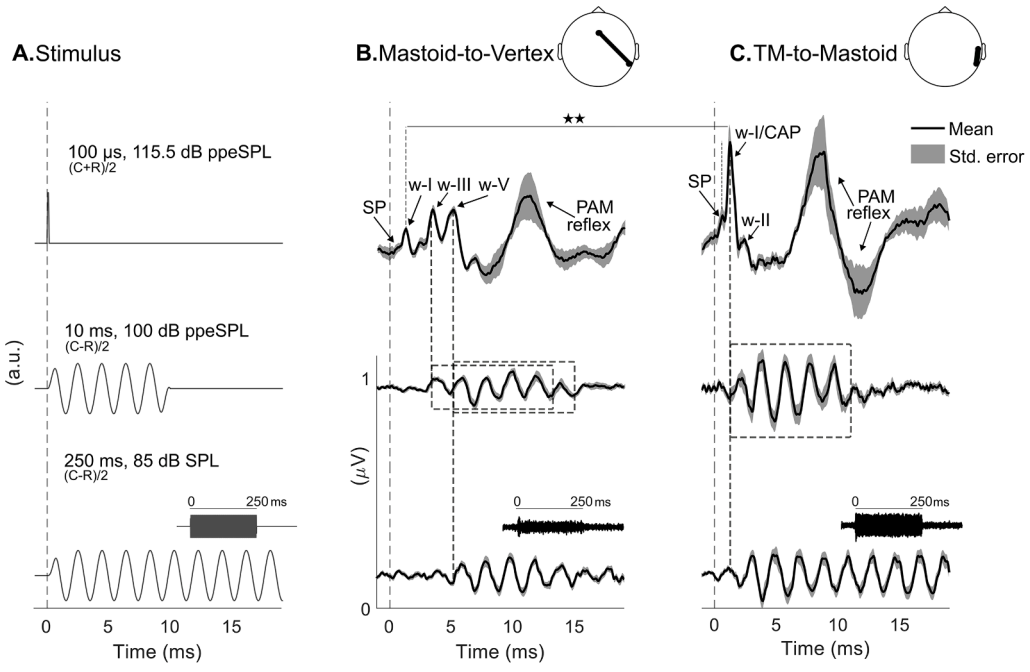

Fig. 1. Stimuli and average simultaneous measurement of ABR and FFR using different electrode configurations. **A**) Waveforms of the three stimuli: 100-μs, 115.5-dB-ppeSPL click (top), 10-ms, 100-dB-ppeSPL pure tone at 516 Hz (middle), and 250-ms, 85-dB-ppeSPL pure tone at 516 Hz (bottom). **B**) Polarity-independent ABR response ((C + R)/2; top) and the polarity-dependent ((C-R)/2) responses to the shorter (middle) and longer (bottom) 516-Hz tone pulses. These responses were collected using the mastoid-to-vertex montage (ipsilateral mastoid-FPz). This configuration captures both peripheral potentials (wave I) and brainstem potentials (waves III and V). The post-auricular muscle (PAM) reflex follows wave V. **C**) Responses obtained with the (ipsilateral) TM-to-mastoid electrode montage. Here, only peripheral potentials are present (i.e., SP, w-I/CAP, w-II). Responses to sustained stimuli reveal isolated ANN activity. Solid lines indicate the average responses of all participants, while shaded areas represent the standard error. ⋆$p < 0.05$, ⋆⋆ $p < 0.01$, ⋆⋆⋆$p < 0.001$.

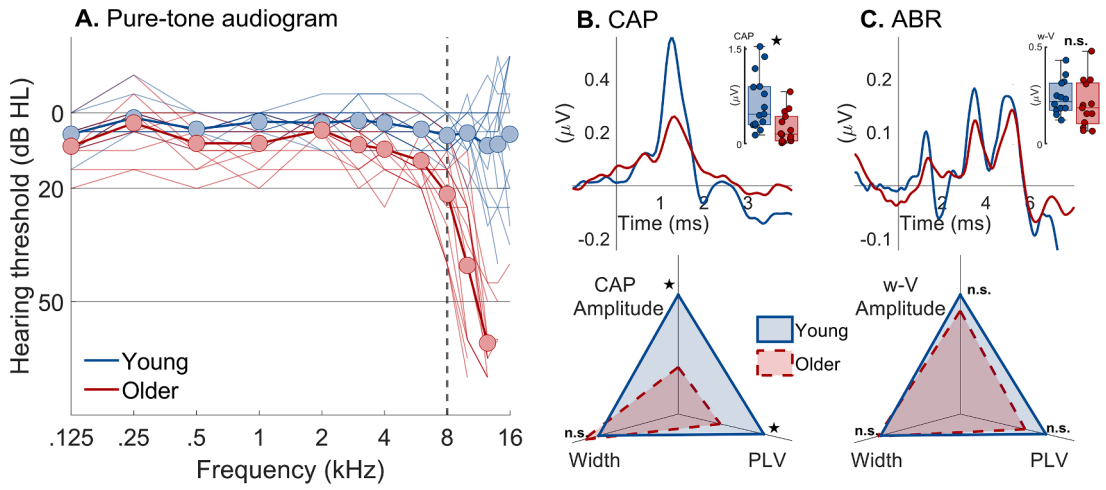

Fig. 2. **A**) Pure-tone thresholds ranging from 125 Hz to 16 kHz for the young (blue) and older (red) participants. The group-average thresholds are shown with thick lines and filled circles, while the individual participants' thresholds are represented with thin lines. **B**) The top panel displays the group-average CAPs elicited by clicks presented at 12 Hz repetition rate for the young (blue) and older (red) participants. The inset shows boxplots of the peak-to-trough amplitudes and individual data points. The bottom panel exhibits a spider diagram presenting CAP amplitude (in μV), onset-to-trough width (in ms), and PLV for the young participants (blue, solid) and the older participants (red, dashed), obtained with the TM-to-mastoid configuration. **C**) The top panel shows the corresponding group-average ABRs to the 12-Hz clicks. The inset displays boxplots of the peak-to-trough amplitude and individual data points. The bottom panel presents a spider diagram illustrating wave-V amplitude, width and PLV, measured with the mastoid-to-vertex configuration.

was the same for both groups. However, the hearing thresholds at 1 kHz and 3 kHz were significantly higher for older listeners than for younger listeners (1 kHz: $t(19.7) = -2.90$, $p = 0.012$; 3 kHz: $t(25.7) = -2.78$, $p = 0.012$).

Consistently, lower DPOAE amplitudes across the F2 range of 500 Hz to 10 kHz were also observed in the older group compared to the young group under the fixed-level condition (65 dB). For frequencies within the clinically-normal threshold range (0.5 to 6 kHz), the averaged DPOAE amplitudes in the older group were significantly lower ($t(21.7) = 3.49$, $p = 0.0042$), consistent with threshold differences in this range. At higher frequencies (8 to 10 kHz), a much lower number of significant DPOAEs were observed across groups and were therefore excluded from statistical analysis (50% and 85.71% of significant responses in the older and young groups, respectively). The DPOAE level-growth functions measured at fixed frequencies (1, 3, 8 and 10 kHz) as a function of stimulation level (40 to 70 dB in steps of 5 dB) confirmed differences in amplitudes between the young and older participants, indicating more shallow DPOAE level-growth in the older participants, consistent with the (small) differences in their pure-tone thresholds.

In Fig. 2B (top panel), the averaged click responses obtained with the TM-to-mastoid montage are presented for the young (blue) and older (red) participants. The CAP amplitude, reflecting compound activity from the AN, was reduced by 60.7% in the older-participant group compared to the young participant group ($t(20.0) = 2.79$, $p = 0.034$). The bottom panel of Fig. 2B) shows a spider diagram illustrating the CAP amplitude (in μV), the onset-to-trough width (in ms), and the PLV. On average, the CAP PLV was reduced by 50.8% in the older group (mean PLV = 0.13 ± 0.0094) compared to the young group (mean PLV = 0.27 ± 0.01; $t(25.8) = 2.80$, $p = 0.034$), indicating reduced synchronized population neural activity at the level of the AN in the older participants. The width of the CAP was not significantly different between the young (mean width = 1.08 ± 0.011 ms) and older participants (mean width = 1.06 ± 0.0314 ms; $t(19.3) = -0.28$, $p = 0.79$). Additionally, we found no differences in SP amplitudes (amplitude-to-baseline) between young and older participants ($t(23) = -0.41$, $p = 0.68$). The differences in CAP amplitude observed here are likely to be influenced by the status of sensory cells in the base of the cochlea.

The top panel of Fig. 2C) shows averaged click responses obtained in the ABR mastoid-to-vertex montage for the young (blue) and older (red) participants. Consistent with the CAP amplitudes, the clinical ABR wave-I amplitude was significantly lower in older listeners compared to younger listeners ($t(24) = 3.47$, $p = 0.002$). The ABR wave-V amplitude was not significantly different for the young and older participants ($t(21.5) = 0.78$, $p = 0.67$). The bottom panel of Fig. 2C) shows a spider diagram depicting ABR wave-V amplitude, onset-to-trough width, and PLV. ABR wave-V PLV and width were also not significantly different in the older group (PLV: 0.08 ± 0.0034; width: 1.79 ± 0.077 ms) compared to the young group (values: PLV: 0.11 ± 0.0037 and width: 1.76 ± 0.068 ms; *t*-tests: PLV: $t(25.8) = 1.70$, $p = 0.2$; and width: $t(24.6) = -0.27$, $p = 0.79$). Furthermore, the absolute CAP (TM-to-mastoid montage) and ABR wave-V (mastoid-to-vertex montage) latencies showed no significant differences between the groups (CAP: $t(17.7) = -1.89$, $p = 0.075$, ABR wave V: $t(25.5) = -1.93$, $p = 0.066$).

3.3. *Responses to longer-duration tone pulses (250 ms, 85 dB SPL)*

Fig. 3 illustrates the responses to the 250-ms tone pulses. In Fig. 3A (left panel), the across-group averaged results for the 516-Hz tone, obtained with the two montages (indicated by the black and gray waveforms), are presented. Fig. 3B (left panel) displays the corresponding results for the 1086-Hz tone. For responses recorded with the mastoid-to-vertex montage, we observed a significant decrease in PLV in the older group compared to the younger group at both stimulation frequencies (516 Hz: $t(26) = 3.46$, $p = 0.0038$, 1086 Hz: $t(26) = 2.84$, $p = 0.026$). Similarly, the SNR of the 516-Hz FFR was also reduced in the older participant group (not shown, $t(20.6) = 3.63$, $p = 0.0038$), whereas the SNR of the FFR at 1086 Hz was *not* statistically different between the groups ($t(19.9) = 2.11$, $p = 0.057$). We found no significant differences between the amplitudes of the response spectra at the frequency of stimulation, or 'spectral amplitudes', at both frequencies (not shown, 516 Hz: $t(19.4) = 2.04$, $p = 0.055$, 1032 Hz: $t(19) = 1.5$, $p = 0.15$).

For the TM-to-mastoid montage, we observed significant group differences in PLV at both stimulation frequencies (516 Hz: $t(26) = 3.86$, $p = 0.0038$, 1086 Hz: $t(26) = 2.86$, $p = 0.026$). Age effects were also significant in terms of the SNR at 516 Hz (not shown, $t(23.2) = 3.33$, $p = 0.0044$). In contrast to the mastoid-to-vertex results, we also observed a significant age-related decrease in SNR at 1086 Hz (not shown, $t(20.2) = 2.35$, $p = 0.043$). Similar age effects were observed for the spectral amplitudes of the TM-to-mastoid montage responses at both stimulation

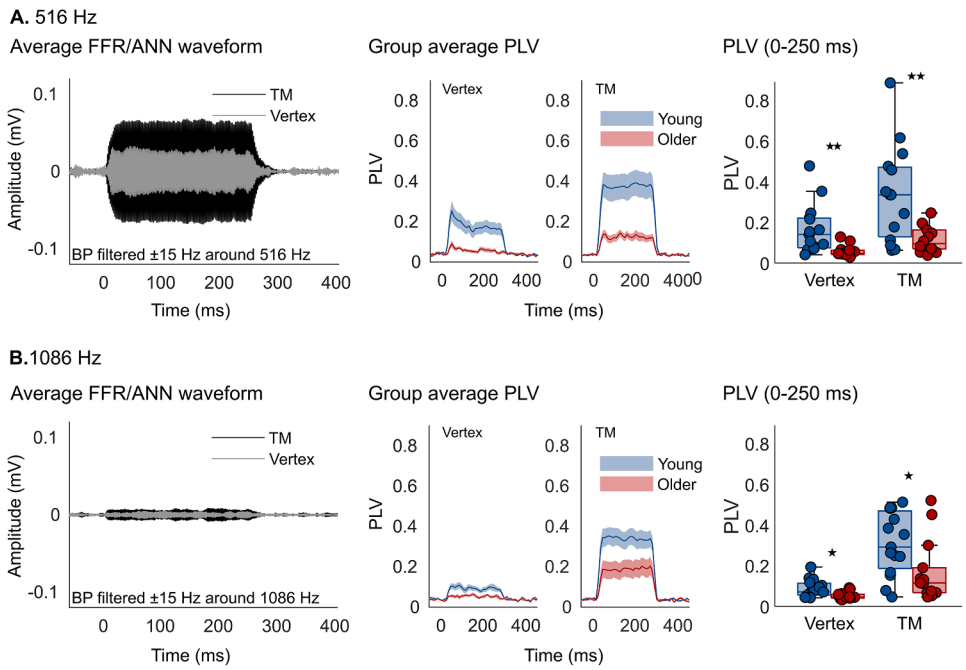

Fig. 3. Average responses to 250-ms tone pulses at 516 Hz (**A**) and 1086 Hz **(B)**, bandpass filtered (+/- 15 Hz), presented at 85 dB SPL. The left panels show the waveforms of the polarity-dependent responses (C-R)/2, averaged across all participants, obtained using the TM-to-mastoid montage (black) and the mastoid-to-vertex montage (gray). The middle panels show the PLV at the stimulation frequency of the young (blue) and the older (red) participants, obtained with the mastoid-to-vertex montage (left) and the TM-to-mastoid montage (right). The shaded areas represent standard errors. The right panels show boxplots of the PLVs to the stimulation frequency, averaged across the interval from 0 to 250 ms, for both montages and participant groups. The individual data points are represented as circles ($\star p < 0.05$, $\star\star\ p < 0.01$, $\star\star\star p < 0.001$).

frequencies (not shown, 516 Hz: t(20.7) = 2.55, $p = 0.022$, 1086 Hz: t (21.1) = 2.54, $p = 0.038$). A summary of the statistics is displayed in Table 1.

The FFR age effects observed here are consistent with those reported in Märcher-Rørsted et al. (2022). Concurrent reduction in ANN in the older listeners further supports the notion that the FFR reduction at lower frequencies (516 Hz) is driven by neural cochlear loss. Yet, although the older participants were recruited to have normal thresholds, subclinical differences in the status of sensory cells could confound these effects. To examine this further, we included low frequency (<6 kHz) thresholds and (<6 kHz) DPOAEs in multivariable linear regression models to adjust for potential age-related differences in measures reflecting the status of apical OHCs. The FFR SNR, measured in the mastoid-to-vertex montage, showed significant effects of age at 516 Hz when adjusting for low-frequency thresholds (t(20) = −2.78, $p = 0.0116$) or DPOAEs (t(19) = −2.407, $p = 0.0264$). SNR of the TM-to-mastoid ANN response at 516 Hz also showed statistical age differences when adjusting for either PTA thresholds (t(23) = −2.185, $p = 0.0393$) or DPOAEs (t(21) = −2.646, $p = 0.0151$), but the 1086-Hz ANN response no longer showed statistically significant age-effects when adjusting for thresholds (t(24) = −1.441, $p = 0.163$) or DPOAEs (t(22) = −1.68, $p = 0.107$). Thresholds at extended high frequencies were very highly correlated with age (r(26) = 0.92, $p <$ 1e-11) and our design does not allow to control for them. However, as argued in Märcher-Rørsted et al. (2022), basal OHCs are likely to have little influence on low-frequency FFRs.

3.4. *Responses to high-intensity tone bursts (10 ms, 100 dB peSPL)*

Fig. 4 presents the average responses to the short (10-ms) high-intensity (100 dB ppeSPL) pure tones at 516 Hz (Fig. 4A), 1032 Hz (Fig. 4B) and 3096 Hz (Fig.4C). The left panels in Fig. 4A, B and C depict the group-averaged waveforms obtained with the mastoid-to-vertex montage (left) and the TM-to-mastoid montage (right) for the young (red) and older (blue) participants. The averaged responses were delay-corrected to visually highlight the amplitude differences in the response patterns across subjects. The 516 and 1032 Hz conditions (Fig. 4A and 4B) represent responses dominated by the neural sources (at cochlear

Table 1
Summary statistics (PLV, SNR, and spectral amplitudes) of the responses to the 250-ms pure tones at 516 and 1086 Hz with the mastoid-to-vertex and TM-to-mastoid electrode configurations.

	Mastoid-to-vertex				TM-to-mastoid			
	df	t	p		df	t	p	
PLV								
516 Hz	(26)	3.46	**0.0038**	★★	(26)	3.86	**0.0038**	★★
1086 Hz	(25)	2.84	**0.026**	★	(26)	2.86	**0.026**	★
SNR								
516 Hz	(20.6)	3.63	**0.0038**	★★	(23.2)	3.33	**0.0044**	★★
1086 Hz	(19.9)	2.11	0.057		(20.2)	2.35	**0.043**	★
Spectral amplitude								
516 Hz	(19.4)	2.04	0.055		(20.7)	2.55	**0.022**	★
1086 Hz	(19)	1.5	0.15		(21.1)	2.54	**0.038**	★

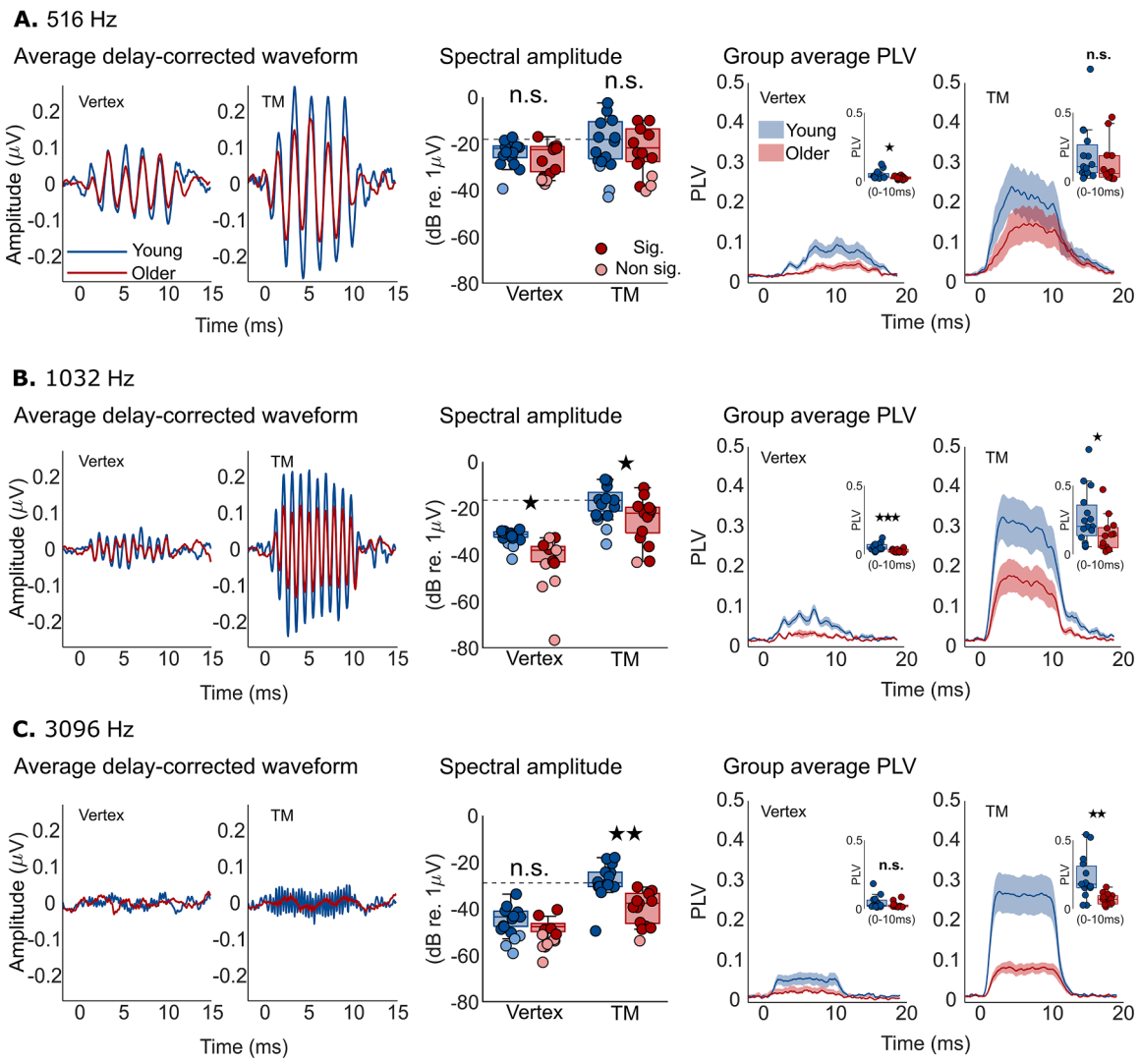

Fig. 4. Averaged responses to the 10-ms tone bursts at 516 Hz (**A**), 1032 Hz (**B**) and 3096 Hz (**C**) at 100 dB ppeSPL. The left panels in **A), B)** and **C)** display the delay-corrected polarity-dependent responses ((C-R)/2) for the young (blue) and older (red) participants, obtained using the mastoid-to-vertex montage (left) and the TM-to-mastoid montage (right) for the respective frequencies. The middle panels in **A), B)** and **C)** depict the corresponding amplitudes of the spectra at the stimulation frequency (spectral amplitude) measured using the mastoid-to-vertex (left) and TM-to-mastoid (right) montages. Dashed lines indicate the median values of the young participants in the TM-to-mastoid montage. The right panels in **A), B)** and **C)** present the PLV to the stimulation frequency measured using the mastoid-to-vertex (left) and TM-to-mastoid (right) montages evaluated in the time interval −2 to 20 ms. The shaded areas represent standard errors.. The inset displays boxplots of the PLVs averaged from 0 to 10 ms for the stimulation frequency. The individual data points are also displayed as circles ($\star p < 0.05$, $\star\star\ p < 0.01$, $\star\star\star p < 0.001$).

and brainstem levels). The 3096-Hz stimulation condition (Fig. 4C) was included to estimate the isolated CM and is described further below.

For the responses obtained with the mastoid-to-vertex electrode montage, we observed a reduction in the PLVs of the older group at 516 Hz ($t(26) = 2.71$, $p = 0.047$, Fig. 4A, right panel) and 1032 Hz ($t(25) = 4.29$, $p = 0.00094$, Fig. 4B, right panel), consistent with the results using the longer tonal stimulation. In contrast to the results obtained with the longer-duration tones, the SNR of the 516 Hz response was not significantly different between the two groups ($t(18.3) = 1.06$, $p = 0.3$, not shown). Significant differences were, however, observed at 1032 Hz ($t(14.1) = 2.91$, $p = 0.011$, not shown). Similarly, the spectral amplitudes of the response for the older group were significantly reduced at 1032 Hz ($t(4.7) = 3.56$, $p = 0.028$, Fig. 4B, middle panel) but not at 516 Hz ($t(12.8) = 0.94$, $p = 0.40$, Fig. 4A, middle panel). It is important to note that only 5 of the 14 older participants showed significant FFRs at 1032 Hz (F-test, see Section 2.3).

For the TM-to-mastoid montage, in contrast to the results with the longer-duration tones, the PLVs of the responses were not significant at 516 Hz ($t(26) = 1.29$, $p = 0.4$, Fig. 4A, right panel). However, significant effects were found in the PLVs at 1032 Hz ($t(25) = 1.19$, $p = 0.038$, Fig. 4B, right), as in the case of the longer duration stimulation. No age effects were observed in the SNRs at either of the frequencies (516 Hz: $t(12.1) = 0.993$, $p = 0.34$; 1032 Hz: $t(20.4) = 1.5$, $p = 0.15$, not shown). Finally, the spectral amplitudes of the older group were significantly reduced at 1032 Hz ($t(21.0) = 2.49$, $p = 0.028$, Fig. 4B, middle panel). We did not find a significant difference in spectral amplitude of the 516 Hz response between the groups ($t(18.9) = 0.87$, $p = 0.40$, Fig. 4A, middle panel). A summary of the statistics of the responses to the 10-ms pure tones can be found in Table 2.

3.5. Estimating the cochlear microphonic (CM)

Fig. 4C illustrates the average response of the two age groups to the 10-ms tone bursts at 3096 Hz. This stimulus condition was included to estimate CM responses, i.e., by stimulating beyond the suspected limit of phase-locking of AN fibers (Dynes and Delgutte, 1992; Johnson, 1980). Significant differences in average PLVs across the age groups were found with the TM electrode ($t(26) = 4.06$, $p = 0.00139$), but not with the

Table 2
Summary statistics (PLV, SNR, and spectral amplitudes) of the responses to the 10-ms pure tones at 516, 1032, and 3096 Hz with the mastoid-to-vertex and TM-to-mastoid electrode configurations.

	Mastoid-to-vertex				TM-to-mastoid			
	df	t	p		df	t	p	
PLV								
516 Hz	(26)	2.71	**0.047**	★	(26)	1.29	0.40	
1032 Hz	(25)	4.27	**<0.001**	★★★	(25)	1.19	**0.038**	★
3096 Hz	(26)	1.73	0.19		(26)	4.06	**0.00139**	★★
SNR								
516 Hz	(18.3)	1.06	0.3		(12.1)	0.99	0.34	
1032 Hz	(14.1)	2.91	**0.011**	★	(20.4)	1.50	0.15	
3096 Hz	(13.8)	0.51	0.62		(21.9)	1.35	0.29	
Spectral amplitude								
516 Hz	(12.8)	0.94	0.4		(18.9)	0.87	0.40	
1032 Hz	(4.7)	3.56	**0.028**	★	(21)	2.49	**0.028**	★
3096 Hz	(9)	0.97	0.43		(24.7)	4.03	**0.00139**	★★

vertex electrode ($t(26) = 1.73$, $p = 0.19$, Fig. 4C, right panel). Similarly, significant differences in spectral amplitudes at 3 kHz between the two age groups were found with the TM-to-mastoid montage ($t(24.7) = 4.03$, $p = 0.00139$, Fig. 4C, middle panel). No effects were observed with the mastoid-to-vertex electrode configuration ($t(9) = 0.97$, $p = 0.43$, Fig. 4C, middle panel). On average, the amplitudes of the responses to the 3-kHz tones were lower than the 500-Hz and 1-kHz condition responses (Fig. 4, left panels). The spectral amplitudes of the young groups were more than 10 dB smaller at 3 kHz than at 500 and 1032 Hz (dashed lines middle panels). The response at 3096 Hz (right) exhibited a relatively flat amplitude pattern over time for both age groups, whereas the responses at 516 Hz and 1032 Hz showed slightly decaying waveform amplitudes and PLV patterns over time, indicating some neural adaptation (see right columns of Fig. 4A, B and C).

4. Discussion

The aim of this study was to explore frequency-following responses to high-intensity low-frequency pure tones as a potential clinical indicator of cochlear neural degeneration. Transient and periodic evoked potentials originating from the cochlea and brainstem were simultaneously recorded in both young and older participants with normal or near-normal clinical audiometric thresholds. Periodic potentials following the carrier of the pure tone stimulation showed a decrease in both ECochG (ANN) and scalp (FFR) electrode montages in the older participants. Significant reductions in responses to clicks were also observed in the peripheral CAP response but not in the brainstem ABR wave V in the older group.

The amplitude of ABR wave I (or the CAP) has been used as a primary electrophysiological marker of noise-induced or age-related CS in non-human animal studies (Bramhall, 2021; Furman et al., 2013; Kujawa and Liberman, 2009; Sergeyenko et al., 2013). Particularly in animal models of noise-induced CS, cochlear synaptic loss can be induced without concomitant loss of hair cells by controlling the duration and intensity of the noise insult. However, in humans, CS is likely to co-occur with other losses (e.g., IHC and OHC loss) (Wu et al., 2019), which may also affect the morphology and the amplitude of ABR wave I (Verhulst et al., 2018), compromising its specificity. Indeed, recent work has suggested that the CAP might be affected by hair cell potentials and that the summating potential (SP) might be affected by neural sources (Vasilkov et al., 2023). This might explain why studies investigating electrophysiological correlates of behavioral measures, such as word recognition, surprisingly report strong correlations with SP rather than of CAP amplitudes (Grant et al., 2020; Lai and Bidelman, 2022). These findings suggest that the peaks in ABRs or ECochG responses to transient sounds may reflect responses from a complex mixture of different cochlear sources and might therefore not be an optimal measure of CS or AN degeneration.

Steady-state evoked potentials have also been proposed as a potential marker of cochlear neural loss (Bharadwaj et al., 2015; Encina-Llamas et al., 2019; Keshishzadeh et al., 2020; Märcher-Rørsted et al., 2022; Parthasarathy and Kujawa, 2018; Prendergast et al., 2019; Shaheen et al., 2015). In a recent study, we showed a reduced magnitude of the brainstem FFR in response to tone stimulation in older humans assumed to present a larger degree of AN degeneration despite near-normal clinical thresholds, (Märcher-Rørsted et al., 2022), consistent with other previous work (Clinard and Cotter, 2015; Mamo et al., 2016; Presacco et al., 2016). Based on simulated AN responses using a computational AN model, Märcher-Rørsted et al. (2022) suggested that the reduced FFR in older listeners could be driven by age-related AN degeneration, despite the fact that the FFR is generated in the auditory brainstem (Henry, 1995; Snyder and Schreiner, 1984).

Here, we have demonstrated that both peripheral ANNs and brainstem FFRs were reduced in older individuals with near-normal clinical thresholds (Figs 3 and 4 and Tables 1 and 2), as predicted by our previous modeling simulations (Märcher-Rørsted et al., 2022). Additionally, we found a significant reduction in CAP and clinical ABR wave-I amplitudes in the older listeners. The reduction of the CAP amplitude in older listeners is consistent with AN degeneration but may also be caused by basal OHC loss (Elberling, 1974). EHF pure-tone thresholds (Fig. 2A) and DPOAE amplitudes at higher frequencies were strongly reduced, and basal OHC loss is likely to be common in older humans (Wu et al., 2019), even if clinical thresholds are relatively normal as in the current study. FFR stimulation using low-frequency tones at relatively high levels produces a broadband excitation across AN fibers which is likely to be minimally affected by basal OHC loss or dysfunction (Encina-Llamas et al., 2019; Märcher-Rørsted et al., 2022). The ANN (or FFR) might thus present an advantage as a marker of neural cochlear degeneration over CAP or ABR wave I amplitudes.

The amplitudes of ABR wave V were statistically similar in young and older listeners (Fig. 2C) while the amplitudes of CAP and wave I (Fig. 2B) were reduced in the older listeners. Previous studies have reported either a similar restoration of wave V amplitudes (Burkard and Sims, 2001; Grose et al., 2019; P. T. Johannesen and Lopez-Poveda, 2021; Rumschlag et al., 2022) or an increase in the ratio of wave V/I amplitudes with age (P. Johannesen et al., 2019; Psatta et al., 1988; Sand, 1991). In contrast, brainstem FFR amplitudes were reduced in the older listeners (Figs. 3 and 4). This suggests that the amplitude of the brainstem response to transient stimuli presented at low stimulation rates was restored in the older listeners, while this is not the case for steady-state responses to pure tones. It has been suggested that a lack of cochlear output due to AN damage may lead to plastic changes throughout the auditory pathway, including hyper-synchronous firing across neural populations (Auerbach et al., 2014; Salvi et al., 2017; Sheppard et al., 2018). These mechanisms have been described as having a bidirectional effect at different rates: showing *enhanced* synchronization in responses

to stimuli at low presentation rates (i.e., clicks at 12 Hz, Goossens et al., 2016; Presacco et al., 2016; Purcell et al., 2004), but *decreased* synchronization to stimulation with higher rates (i.e., 500 and 1000 Hz, Anderson et al., 2012; Purcell et al., 2004 see also review Herrmann and Butler, 2021). Our results are consistent with rate-dependent hyper--synchronous activity.

Pre-synaptic hair cell potentials (i.e., the CM) in response to low-frequency, high-intensity pure tones can be superimposed to the ANN. It has been argued that the main contributors to the CM are passively-activated high-frequency basal OHCs (Snyder and Schreiner, 1984). Since there might be a large difference in basal OHC status between the young and the older listeners (Fig. 2A), reduced CM responses in older listeners were expected. If the magnitude of the CM is comparable to the magnitude of the ANN at the TM electrode, this may present a limitation to the current approach. To estimate the magnitude of the CM recorded with the TM electrode, we used a high-frequency tone (3 kHz). It can be assumed that phase-locked neural responses from both the AN (the ANN) and the brainstem (the FFR) are negligible at this frequency (Snyder and Schreiner, 1984; Worden and Marsh, 1968). As expected, we observed a significant age-related effect with lower response amplitudes in the older group (Fig. 4C and Table 2), consistent with reduced OAE amplitudes and elevated hearing thresholds (Fig 2A). Previous studies have shown that the magnitude of the CM measured from the round window is relatively constant across stimulation frequency (Snyder and Schreiner, 1984, their Fig. 11). Thus, we assumed that the CM amplitude recorded from the TM electrode with the 3 kHz tone (−29 dB rel. 1 μV in the young listeners, Fig. 4C) would correspond to the CM contribution to the overall response recorded at the low (516 Hz) and mid (1032 kHz) frequency tones. The magnitude of the CM estimated with the 3 kHz pure tones was also significantly smaller than the magnitudes (the sum of the CM and ANN) recorded at 516 Hz and 1032 Hz. Given that the estimated CM magnitude was more than 10 dB smaller than the total ANN magnitudes (Fig. 4, middle panels, dashed lines), we conclude that the responses at the lower frequencies mainly reflect neurophonic responses. Nevertheless, it is possible that the CM measured from the TM, as opposed to the round window, is attenuated at higher frequencies, and the contribution at 0.5 and 1 kHz might have been larger than the estimated CM amplitude using the 3 kHz tone. Moreover, the possibility of a contribution of the reduced CM response to the age-related effects observed at lower frequencies cannot be ruled out. To counter this possibility, it was found that the amplitudes of the transient-evoked SP did not significantly differ between the two groups. However, it is important to note that some of the SP's energy might have been filtered out by the 100 Hz high-pass filter integrated in the recording system. A more detailed examination of the energy composition of the different SP (and CAP) components is necessary if they are to be used as indicators of neural degeneration, given the complexity of sources contributing to these responses (Lutz et al., 2022).

Recent research in gerbils and human round window-ECochG concluded that, at high SPLs, the proportion of ANN present in the total response (CM + ANN) is less than 40% (Haggerty et al., 2023). While most of the ANN's energy is found at the 1st harmonic, it has been proposed that responses at higher harmonics primarily correspond to the ANN (although at high SPLs the saturation of the CM can also contribute to the 2nd harmonic). We examined the 2nd (in the (C + R)/2 polarity) and the 3rd harmonics (in the (C-R)/2 polarity) and found a trend of lower amplitudes and SNRs in the older participants (not shown). However, the age differences were not significant, possibly due to the low number of significant harmonics in the older (48.2%) compared to young (71.4%) participants. Despite this, we interpret this degraded harmonic content in the ANN in the older participants as consistent with AN degeneration. To further investigate CM contamination, experimental paradigms designed to isolate the contribution of the CM at lower frequencies should be considered. The use of amplitude-modulated stimuli eliciting responses to the stimulus envelope and recorded with ECochG may be an alternative approach (Chen and Jennings, 2022). Another approach has been to attempt to remove the CM using a high-passed noise masker, as the CM mainly originates from high-CF regions of the cochlea (Carcagno and Plack, 2020).

Furthermore, a potential limitation of using the FFR as a diagnostic marker of neural loss is that a concomitant loss of OHCs at the frequency of the tonal stimulation (i.e., on-frequency, apical OHCs) might reduce the amplitude of the neural potentials (i.e., the ANN and FFR). In this study, older participants were selected to have a negligible threshold elevation at the FFR frequencies, such that this was not a confounding factor. However, in general, older individuals might exhibit a certain degree of low-frequency hearing loss, which could potentially complicate the FFR as a measure of AN degeneration in clinical practice. Yet, human histopathological data showed that an age-related loss of apical OHCs (70–90% from the base) is less extreme than at more basal regions (0–40% from the base). Importantly, the effect of OHC loss at apical audiometric thresholds is much smaller than at basal audiometric frequencies (Wu et al., 2020) due to the limited cochlear gain at lower frequencies. Consistent with this, modeling work showed that low-frequency OHC loss leading to about a 40 dB hearing threshold shift did not significantly reduce the ANN (Märcher-Rørsted et al., 2022). Overall, the FFR seems to be a potentially valuable biomarker for AN degeneration, being relatively unaffected by both off-frequency basal OHC loss and on-frequency apical OHC loss.

5. Conclusion

The present study investigated potential age-related neural degeneration in the cochlea using ECochG and EEG. It was observed that both the cochlear ANN and brainstem FFR amplitudes to sustained tone stimulation were reduced with age, whereas click-evoked ABR wave V from similar brainstem sources was not affected. This is consistent with the notion that the age-related reduction of the brainstem FFR is mainly driven by age-related ANF loss. The FFR may serve as a valuable tool for assessing ANF status in humans.

CRediT authorship contribution statement

Miguel Temboury-Gutierrez: Writing – review & editing, Writing – original draft, Visualization, Validation, Supervision, Software, Project administration, Methodology, Investigation, Formal analysis, Data curation, Conceptualization. **Jonatan Märcher-Rørsted:** Writing – review & editing, Writing – original draft, Visualization, Validation, Supervision, Software, Project administration, Methodology, Investigation, Formal analysis, Conceptualization. **Michael Bille:** Writing – review & editing, Methodology, Investigation. **Jesper Yde:** Methodology, Investigation, Writing – review & editing. **Gerard Encina-Llamas:** Writing – review & editing, Writing – original draft, Validation, Supervision, Project administration, Methodology, Investigation, Conceptualization. **Jens Hjortkjær:** Writing – review & editing, Writing – original draft, Supervision, Project administration, Methodology, Investigation, Funding acquisition, Conceptualization. **Torsten Dau:** Writing – review & editing, Writing – original draft, Supervision, Project administration, Methodology, Investigation, Funding acquisition, Conceptualization.

Declaration of competing interest

None.

Data availability

Data will be made available on request.

Acknowledgments

This work was supported by the Novo Nordisk Foundation synergy grant NNF17OC0027872 (UHeal), the Oticon center of Excellence for Hearing and Speech Sciences (CHeSS), the center for Auditory Neuroscience (CAN) and the GN Foundation (grant 237).

References

Anderson, S., Parbery-Clark, A., White-Schwoch, T., Kraus, N., 2012. Aging affects neural precision of speech encoding. J. Neurosci. 32 (41), 14156–14164. https://doi.org/10.1523/JNEUROSCI.2176-12.2012.

Auerbach, B.D., Rodrigues, P.V., Salvi, R.J., 2014. Central gain control in tinnitus and hyperacusis. Front. Neurol. 5 https://doi.org/10.3389/fneur.2014.00206.

Benjamini, Y., Hochberg, Y., 1995. Controlling the false discovery rate: a practical and powerful approach to multiple testing. J. R. Stat. Soc.: Ser. B (Methodological) 57 (1), 289–300. https://doi.org/10.1111/j.2517-6161.1995.tb02031.x.

Bharadwaj, H.M., Masud, S., Mehraei, G., Verhulst, S., Shinn-Cunningham, B.G., 2015. Individual differences reveal correlates of hidden hearing deficits. J. Neurosci. 35 (5), 2161–2172. https://doi.org/10.1523/JNEUROSCI.3915-14.2015.

Bidelman, G.M., 2015. Multichannel recordings of the human brainstem frequency-following response: scalp topography, source generators, and distinctions from the transient ABR. Hear. Res. 323, 68–80. https://doi.org/10.1016/j.heares.2015.01.011.

Bourien, J., Tang, Y., Batrel, C., Huet, A., Lenoir, M., Ladrech, S., Desmadryl, G., Nouvian, R., Puel, J.-L., Wang, J., 2014. Contribution of auditory nerve fibers to compound action potential of the auditory nerve. J. Neurophysiol. 112, 1025–1039. https://doi.org/10.1152/jn.00738.2013.-Sound-evoked.

Bramhall, N., Beach, E.F., Epp, B., Le Prell, C.G., Lopez-Poveda, E.A., Plack, C.J., Schaette, R., Verhulst, S., Canlon, B., 2019. The search for noise-induced cochlear synaptopathy in humans: mission impossible? Hear. Res. 377, 88–103. https://doi.org/10.1016/j.heares.2019.02.016.

Bramhall, N.F., 2021. Use of the auditory brainstem response for assessment of cochlear synaptopathy in humans. J. Acoust. Soc. Am. 150 (6), 4440–4451. https://doi.org/10.1121/10.0007484.

Burkard, R.F., Sims, D., 2001. The human auditory brainstem response to high click rates. Am. J. Audiol. 10 (2), 53–61. https://doi.org/10.1044/1059-0889(2001/008.

Carcagno, S., Plack, C.J., 2020. Effects of age on electrophysiological measures of cochlear synaptopathy in humans. Hear. Res. 396 https://doi.org/10.1016/j.heares.2020.108068.

Chen, J., Jennings, S.G., 2022. Temporal envelope coding of the human auditory nerve inferred from electrocochleography: comparison with envelope following responses. J. Assoc. Res. Otolaryngol. https://doi.org/10.1007/s10162-022-00865-z.

Clinard, C.G., Cotter, C.M., 2015. Neural representation of dynamic frequency is degraded in older adults. Hear. Res. 323, 91–98. https://doi.org/10.1016/j.heares.2015.02.002.

Clinard, C.G., Tremblay, K.L., Krishnan, A.R., 2010. Aging alters the perception and physiological representation of frequency: evidence from human frequency-following response recordings. Hear. Res. 264 (1–2), 48–55. https://doi.org/10.1016/j.heares.2009.11.010.

Dau, T., 2003. The importance of cochlear processing for the formation of auditory brainstem and frequency following responses. J. Acoust. Soc. Am. 113 (2), 936–950. https://doi.org/10.1121/1.1534833.

Dau, T., Wegner, O., Mellert, V., Kollmeier, B., 2000. Auditory brainstem responses with optimized chirp signals compensating basilar-membrane dispersion. J. Acoust. Soc. Am. 107 (3), 1530–1540. https://doi.org/10.1121/1.428438.

Delorme, A., Makeig, S., 2004. EEGLAB: an open source toolbox for analysis of single-trial EEG dynamics including independent component analysis. J. Neurosci. Methods 134 (1), 9–21. https://doi.org/10.1016/J.JNEUMETH.2003.10.009.

Dobie, R.A., Wilson, M.J., 1996. A comparison of *t*-test, F test, and coherence methods of detecting steady-state auditory-evoked potentials, distortion-product otoacoustic emissions, or other sinusoids. J. Acoust. Soc. Am. 100 (4), 2236–2246. https://doi.org/10.1121/1.417933.

Dynes, S.B.C., Delgutte, B., 1992. Phase-locking of auditory-nerve discharges to sinusoidal electric stimulation of the cochlea. Hear. Res. 58 (1), 79–90. https://doi.org/10.1016/0378-5955(92)90011-B.

Elberling, C., 1974. Action potentials along the cochlear partition recorded from the Ear Canal in Man. Scand Audiol 3 (1), 13–19. https://doi.org/10.3109/01050397409044959.

Encina-Llamas, G., Harte, J.M., Dau, T., Shinn-Cunningham, B., Epp, B., 2019. Investigating the effect of cochlear Synaptopathy on envelope following responses using a model of the auditory nerve. JARO - J. Assoc. Res. Otolaryngol. 20 (4), 363–382. https://doi.org/10.1007/s10162-019-00721-7.

Ferraro, J., 1998. Electrocochleography. Curr. Opin. Otolaryngol. Head Neck. Surg. 6 (5), 338–341. https://doi.org/10.1097/00020840-199810000-00011.

Furman, A.C., Kujawa, S.G., Liberman, M.C., 2013. Noise-induced cochlear neuropathy is selective for fibers with low spontaneous rates. J. Neurophysiol. 110, 577–586. https://doi.org/10.1152/jn.00164.2013.-Acoustic.

Gardi, J., Merzenich, M., Mckean, C., 1979. Origins of the scalp-recorded frequency-following response in the cat. Int. J. Audiol. 18 (5), 353–380. https://doi.org/10.3109/00206097909070062.

Garrett, M., Verhulst, S., 2019. Applicability of subcortical EEG metrics of synaptopathy to older listeners with impaired audiograms. Hear. Res. 380, 150–165. https://doi.org/10.1016/j.heares.2019.07.001.

Goossens, T., Vercammen, C., Wouters, J., van Wieringen, A., 2016. Aging affects neural synchronization to speech-related acoustic modulations. Front. Aging Neurosci. 8 (JUN) https://doi.org/10.3389/fnagi.2016.00133.

Grant, K.J., Mepani, A.M., Wu, P., Hancock, K.E., Gruttola, V.De, Liberman, M.C., Maison, S.F, 2020. Electrophysiological markers of cochlear function correlate with hearing-innoise performance among audiometrically normal subjects. J. Neurophysiol. 124 (2), 418–431. https://doi.org/10.1152/jn.00016.2020.

Grose, J.H., Buss, E., Elmore, H., 2019. Age-related changes in the auditory brainstem response and suprathreshold processing of temporal and spectral modulation. Trends Hear. 23 https://doi.org/10.1177/2331216519839615.

Guest, H., Munro, K.J., Prendergast, G., Howe, S., Plack, C.J., 2017. Tinnitus with a normal audiogram: relation to noise exposure but no evidence for cochlear synaptopathy. Hear. Res. 344, 265–274. https://doi.org/10.1016/J.HEARES.2016.12.002.

Haggerty, R.A., Hutson, K.A., Riggs, W.J., Brown, K.D., Pillsbury, H.C., Adunka, O.F., Buchman, C.A., Fitzpatrick, D.C., 2023. Assessment of cochlear synaptopathy by electrocochleography to low frequencies in a preclinical model and human subjects. Front. Neurol. 14 https://doi.org/10.3389/fneur.2023.1104574.

Harris, K.C., Ahlstrom, J.B., Dias, J.W., Kerouac, L.B., McClaskey, C.M., Dubno, J.R., Eckert, M.A., 2021. Neural presbyacusis in humans inferred from age-related differences in auditory nerve function and structure. J. Neurosci.: Off. J. Soc. Neurosci. 41 (50), 10293–10304. https://doi.org/10.1523/JNEUROSCI.1747-21.2021.

Hecox, K., Galambos, R., 1974. Brain stem auditory evoked responses in human infants and adults. Arch. Otolaryngol. - Head Neck Surg. 99 (1), 30–33. https://doi.org/10.1001/archotol.1974.00780030034006.

Henry, K.R., 1995. Auditory nerve neurophonic recorded from the round window of the Mongolian gerbil. Hear. Res. 90 (1–2), 176–184. https://doi.org/10.1016/0378-5955(95)00162-6.

Herrmann, B., Butler, B.E., 2021. Hearing loss and brain plasticity: the hyperactivity phenomenon. In: Brain Structure and Function, 226. Springer Science and Business Media Deutschland GmbH, pp. 2019–2039. https://doi.org/10.1007/s00429-021-02313-9.

Hickox, A.E., Larsen, E., Heinz, M.G., Shinobu, L., Whitton, J.P., 2017. Translational issues in cochlear synaptopathy. In: Hearing Research, 349. Elsevier B.V, pp. 164–171. https://doi.org/10.1016/j.heares.2016.12.010.

Jerger, J., Johnson, K., 1988. Interactions of age, gender, and sensorineural hearing loss on ABR latency. Ear. Hear. 9 (4), 168–176. https://doi.org/10.1097/00003446-198808000-00002.

Johannesen, P., Buzo, B., Lopez-Poveda, E., 2019. Evidence for age-related cochlear synaptopathy in humans unconnected to speech-in-noise intelligibility deficits. Hear. Res. 374 https://doi.org/10.1016/j.heares.2019.01.017.

Johannesen, P., Lopez-Poveda, E., 2021. Age-related central gain compensation for reduced auditory nerve output for people with normal audiograms, with and without tinnitus. iScience 24 (6). https://doi.org/10.1016/j.isci.2021.102658.

Johnson, D.H., 1980. The relationship between spike rate and synchrony in responses of auditory-nerve fibers to single tones. J. Acoustic. Soc. Am. 68 (4), 1115–1122. https://doi.org/10.1121/1.384982</bib.

Johnson, T., Brown, C., 2005. Threshold prediction using the auditory steady-state response and the tone burst auditory brain stem response: a within-subject comparison. Ear. Hear. 26 (6), 559–576.

Keshishzadeh, S., Garrett, M., Vasilkov, V., Verhulst, S., 2020. The derived-band envelope following response and its sensitivity to sensorineural hearing deficits. Hear. Res. 392. https://doi.org/10.1016/j.heares.2020.107979.

Keshishzadeh, S., Garrett, M., Verhulst, S., 2021. Towards personalized auditory models: predicting individual sensorineural hearing-loss profiles from recorded human auditory physiology. Trends Hear. 25 https://doi.org/10.1177/2331216520988406.

Kiang, N.Y.S., 1965. Stimulus coding in the auditory nerve and cochlear nucleus. Acta Otolaryngol. 59 (2–6), 186–200. https://doi.org/10.3109/00016486509124552.

King, A., Hopkins, K., Plack, C.J., 2016. Differential group delay of the frequency following response measured vertically and horizontally. JARO - J. Assoc. Res. Otolaryngol. 17 (2), 133–143. https://doi.org/10.1007/s10162-016-0556-x.

Krishnan, A., Mcdaniel, S.S., 1998. Binaural interaction in the human frequency-following response: effects of interaural intensity difference. In: Audiol Neurootol, 3. http://BioMedNet.com/karger.

Kujawa, S.G., Liberman, M.C., 2009. Adding insult to injury: cochlear nerve degeneration after "temporary" noise-induced hearing loss. J. Neurosci. 29 (45), 14077–14085. https://doi.org/10.1523/JNEUROSCI.2845-09.2009.

Lai, J., Bidelman, G.M., 2022. Relative changes in the cochlear summating potentials to paired-clicks predict speech-in-noise perception and subjective hearing acuity. JASA Express. Lett. 2 (10), 102001 https://doi.org/10.1121/10.0014815.

Liberman, M.C., Epstein, M.J., Cleveland, S.S., Wang, H., Maison, S.F., 2016. Toward a differential diagnosis of hidden hearing loss in humans. PLoS ONE 11 (9). https://doi.org/10.1371/JOURNAL.PONE.0162726.

Liberman, M.C., Kujawa, S.G., 2017. Cochlear synaptopathy in acquired sensorineural hearing loss: manifestations and mechanisms. In: Hearing Research, 349. Elsevier B. V., pp. 138–147. https://doi.org/10.1016/j.heares.2017.01.003

Lightfoot, G.R., 1993. Correcting for factors affecting ABR wave V latency. Br. J. Audiol. 27 (3), 211–220. https://doi.org/10.3109/03005369309076695.

Liu, L.F., Palmer, A.R., Wallace, M.N., 2006. Phase-locked responses to pure tones in the inferior colliculus. J. Neurophysiol. 95 (3), 1926–1935. https://doi.org/10.1152/jn.00497.2005.

Lobarinas, E., Salvi, R., Ding, D., 2013. Insensitivity of the audiogram to carboplatin induced inner hair cell loss in chinchillas. Hear. Res. 302, 113–120. https://doi.org/10.1016/j.heares.2013.03.012.

Lopez-Calderon, J., Luck, S.J., 2014. ERPLAB: an open-source toolbox for the analysis of event-related potentials. Front. Hum. Neurosci. 8 (1 APR). https://doi.org/10.3389/fnhum.2014.00213</bib.

Lutz, B.T., Hutson, K.A., Trecca, M.C., Hamby, M., Fitzpatrick, D.C., 2022. Neural contributions to the cochlear summating potential: spiking and dendritic components. J. Assoc. Res. Otolaryngolo. 23 (3), 351–363. https://doi.org/10.1007/s10162-022-00842-6.

Mamo, S.K., Grose, J.H., Buss, E., 2016. Speech-evoked ABR: effects of age and simulated neural temporal jitter. Hear. Res. 333, 201–209. https://doi.org/10.1016/j.heares.2015.09.005.

Märcher-Rørsted, J., Encina-Llamas, G., Dau, T., Liberman, M.C., Wu, P.zhe, Hjortkjær, J., 2022. Age-related reduction in frequency-following responses as a potential marker of cochlear neural degeneration. Hear. Res. 414, 108411 https://doi.org/10.1016/J.HEARES.2021.108411.

Marmel, F., Linley, D., Carlyon, R.P., Gockel, H.E., Hopkins, K., Plack, C.J., 2013. Subcortical neural synchrony and absolute thresholds predict frequency discrimination independently. JARO - J. Assoc. Res. Otolaryngol. 14 (5), 757–766. https://doi.org/10.1007/s10162-013-0402-3.

Mehraei, G., Hickox, A.E., Bharadwaj, H.M., Goldberg, H., Verhulst, S., Charles Liberman, M., Shinn-Cunningham, B.G., 2016. Auditory brainstem response latency in noise as a marker of cochlear synaptopathy. J. Neurosci. 36 (13), 3755–3764. https://doi.org/10.1523/JNEUROSCI.4460-15.2016.

Møller, A.R., Jannetta, P.J., Sekhar, L.N., 1988. Contributions from the auditory nerve to the brain-stem auditory evoked potentials (BAEPs): results of intracranial recording in man. Electroencephalogr. Clin. Neurophysiol./Evoked Potential. Sect. 71 (3), 198–211. https://doi.org/10.1016/0168-5597(88)90005-6.

Moosavi, A., Nazeri, A.R., Lotfi, Y., Bakhshi, E., 2016. Comparison of auditory evoked potentials between younger and older adults. In: Journal of Hearing Sciences and Otolaringology, 2. www.journalhso.com.

Oostenveld, R., Fries, P., Maris, E., Schoffelen, J.-M., 2011. FieldTrip: open source software for advanced analysis of MEG, EEG, and invasive electrophysiological data. Comput. Intell. Neurosci. 2011, 1–9. https://doi.org/10.1155/2011/156869.

Parthasarathy, A., Kujawa, S.G., 2018. Synaptopathy in the aging cochlea: characterizing early-neural deficits in auditory temporal envelope processing. J. Neurosci. 38 (32), 7108–7119. https://doi.org/10.1523/JNEUROSCI.3240-17.2018.

Pérez-González, D., Malmierca, M.S., 2014. Adaptation in the auditory system: an overview. In: Frontiers in Integrative Neuroscience, 8. https://doi.org/10.3389/fnint.2014.00019.

Pichora-Fuller, M.K., Schneider, B.A., MacDonald, E., Pass, H.E., Brown, S., 2007. Temporal jitter disrupts speech intelligibility: a simulation of auditory aging. Hear. Res. 223 (1–2), 114–121. https://doi.org/10.1016/J.HEARES.2006.10.009.

Prendergast, G., Couth, S., Millman, R.E., Guest, H., Kluk, K., Munro, K.J., Plack, C.J., 2019. Effects of age and noise exposure on proxy measures of cochlear synaptopathy. Trends Hear. 23 https://doi.org/10.1177/2331216519877301.

Presacco, A., Simon, J.Z., Anderson, S., 2016. Evidence of degraded representation of speech in noise, in the aging midbrain and cortex. J. Neurophysiol. 116, 2346–2355. https://doi.org/10.1152/jn.00372.2016.-Humans.

Psatta, D.M., Matei, M., Psatta, D.M., 1988. Age-dependent amplitude variation of brain-stem auditory evoked potentials. In: Electroencephalography and Clinical Neurophysiology, 71.

Purcell, D.W., John, S.M., Schneider, B.A., Picton, T.W., 2004. Human temporal auditory acuity as assessed by envelope following responses. J. Acoust. Soc. Am. 116 (6), 3581–3593. https://doi.org/10.1121/1.1798354.

Robert Frisina, D., Frisina, R.D., 1997. Speech recognition in noise and presbycusis: relations to possible neural mechanisms. Hear. Res. 106 (1–2), 95–104. https://doi.org/10.1016/S0378-5955(97)00006-3.

Ruan, Q., Ma, C., Zhang, R., Yu, Z., 2014. Current status of auditory aging and anti-aging research. In: Geriatrics and Gerontology International, 14, pp. 40–53. https://doi.org/10.1111/ggi.12124.

Rumschlag, J.A., McClaskey, C.M., Dias, J.W., Kerouac, L.B., Noble, K.V., Panganiban, C., Lang, H., Harris, K.C., 2022. Age-related central gain with degraded neural synchrony in the auditory brainstem of mice and humans. Neurobiol. Aging 115, 50–59. https://doi.org/10.1016/J.NEUROBIOLAGING.2022.03.014.

Ryan, A., Dallos, P., 1975. Effect of absence of cochlear outer hair cells on behavioural auditory threshold. Nature 253 (1), 44–46.

Salvi, R., Sun, W., Ding, D., Chen, G.Di, Lobarinas, E., Wang, J., Radziwon, K., Auerbach, B.D, 2017. Inner hair cell loss disrupts hearing and cochlear function leading to sensory deprivation and enhanced central auditory gain. In: Frontiers in Neuroscience, 10. Frontiers Media S.A. https://doi.org/10.3389/fnins.2016.00621

Sand, T., 1991. BAEP amplitudes and amplitude ratios: relation to click polarity, rate, age and sex. Electroencephalogr. Clin. Neurophysiol. 78.

Schneider, B., Speranza, F., Pichora-Fuller, M.K., 1998. Age-related changes in temporal resolution: envelope and intensity effects. Canad. J. Exp. Psychol. /Revue Canadienne de Psychologie Expérimentale 52 (4), 184–191. https://doi.org/10.1037/h0087291.

Schuknecht, H.F., Woellner, R.C., 1955. An experimental and clinical study of deafness from lesions of the cochlear nerve. J. Laryngol. Otol. 69 (2), 75–97. https://doi.org/10.1017/S0022215100050465.

Sergeyenko, Y., Lall, K., Charles Liberman, M., Kujawa, S.G., 2013. Age-related cochlear synaptopathy: an early-onset contributor to auditory functional decline. J. Neurosci. 33 (34), 13686–13694. https://doi.org/10.1523/JNEUROSCI.1783-13.2013.

Shaheen, L.A., Valero, M.D., Liberman, M.C., 2015. Towards a diagnosis of cochlear neuropathy with envelope following responses. JARO - J. Assoc. Res. Otolaryngol. 16 (6), 727–745. https://doi.org/10.1007/s10162-015-0539-3.

Sheppard, A., Liu, X., Ding, D., Salvi, R., 2018. Auditory central gain compensates for changes in cochlear output after prolonged low-level noise exposure. Neurosci. Lett. 687, 183–188. https://doi.org/10.1016/j.neulet.2018.09.054.

Smith, S.B., Lichtenhan, J., Cone, B., 2016. Behavioral pure-tone threshold shifts caused by tympanic membrane electrodes. Ear Hear. 37 (4), e273–e275. https://doi.org/10.1097/AUD.0000000000000275.

Snyder, R.L., Schreiner, C.E., 1984. The Auditory Neurophonic: Basic Properties. https://doi.org/10.1016/0378-5955(84)90033-9.

Steinhoff, H.J., Bfhnke, F., Janssen, T., 1988. Oto-Rhino-Laryngology Click ABR intensity-latency characteristics in diagnosing conductive and cochlear hearing losses. In: Arch Otorhinolaryngol, 245.

Sumner, C.J., Palmer, A.R., 2012. Auditory nerve fibre responses in the ferret. Eur. J. Neurosci. 36 (4), 2428–2439. https://doi.org/10.1111/j.1460-9568.2012.08151.x.

Vander Werff, K.R., Burns, K.S., 2011. Brain stem responses to speech in younger and older adults. Ear Hear. 32 (2), 168–180. https://doi.org/10.1097/AUD.0b013e3181f534b5.

Vasilkov, V., Liberman, M.C., Maison, S.F., 2023. Isolating auditory-nerve contributions to electrocochleography by high-pass filtering: a better biomarker for cochlear nerve degeneration? JASa Express. Lett. 3 (2), 024401 https://doi.org/10.1121/10.0017328.

Verhulst, S., Altoè, A., Vasilkov, V., 2018. Computational modeling of the human auditory periphery: auditory-nerve responses, evoked potentials and hearing loss. In: Hearing Research, 360. Elsevier B.V., pp. 55–75. https://doi.org/10.1016/j.heares.2017.12.018

Worden, F.G., Marsh, J.T., 1968. Frequency-following (microphonic-like) neural responses evoked by sound. Electroencephalogr. Clin. Neurophysiol. 25 (1), 42–52. https://doi.org/10.1016/0013-4694(68)90085-0.

Wu, P., Liberman, L., O'Malley, J., Liberman, M., Bennett, K., deGruttola, V., 2019. Primary neural degeneration in the human cochlea: evidence for hidden hearing loss in the aging ear. Neuroscience 407. https://doi.org/10.1016/j.neuroscience.2018.07.053.

Wu, P., O'Malley, J.T., de Gruttola, V., Liberman, M.C., 2020. Age-related hearing loss is dominated by damage to inner ear sensory cells, not the cellular battery that powers them. J. Neurosci. 40 (33), 6357–6366. https://doi.org/10.1523/jneurosci.0937-20.2020.

Wu, P.Z., O'Malley, J.T., de Gruttola, V., Liberman, M.C, 2021. Primary neural degeneration in noise-exposed human cochleas: correlations with outer hair cell loss and word-discrimination scores. J. Neurosci. 41 (20), 4439–4447. https://doi.org/10.1523/JNEUROSCI.3238-20.2021.